A Positive Feedback between Growth and Polarity Provides Directional Persistency and Flexibility to the Process of Tip Growth

Armin Haupt, Dmitry Ershov, Nicolas Minc

A POSITIVE FEEDBACK BETWEEN GROWTH AND POLARITY PROVIDES DIRECTIONAL PERSISTENCY AND FLEXIBILITY TO THE PROCESS OF TIP GROWTH

Armin Haupt[1], Dmitry Ershov[1,2] and Nicolas Minc[1,*,$]

Affiliations:

[1]Institut Jacques Monod, CNRS UMR7592 and Université Paris Diderot, 15 rue Hélène Brion, 75205 Paris Cedex 13, France

[2]Image Analysis Hub at Institut Pasteur, 25-28 Rue du Dr Roux, 75015 Paris.

*Correspondence to: nicolas.minc@ijm.fr (N.M)

[$] Lead contact

KEYWORDS

Cell polarity, Cell growth, Fission Yeast, Fungal Hyphae, Mechanobiology

SUMMARY

Polar cell growth is a conserved morphogenetic process needed for survival, mating, and infection [1, 2]. It typically implicates the assembly and spatial stabilization of a cortical polar domain of the active form of a small GTPase of the Rho family, such as Cdc42, which promotes cytoskeleton assembly and secretion needed for local surface expansion [3-6]. In multiple physiological instances, polarity domains may switch from being spatially unstable exhibiting a wandering behavior around the cell surface, to being stable at a fixed cellular location [7-11]. In here, we show that the rate of surface growth may be a key determinant in controlling the spatial stability of active-Cdc42 domains. Reducing the growth rate of single rod-shaped fission yeast cells using chemical, genetic and mechanical means, systematically causes polar domains to detach from cell tips and oscillate around the cell surface within minutes. Conversely, an abrupt increase in growth rate improves domain stabilization. A candidate screen identifies vesicular transport along actin cables as an important module mediating this process. Similar behavior observed in distant filamentous fungi suggests that this positive feedback between growth and polarity could represent a basal property of eukaryotic polarization promoting persistent polar growth as well as growth redirection with respect to the mechanical environment of cells.

RESULTS AND DISCUSSION

Single cell manipulation of growth rate impacts the stability of GTP-Cdc42 polarity.

Polar domains of the active-form of the Rho-like GTPase Cdc42 promote local growth. Studies in yeast and fungal cells have shown that polar domains can oftentimes become unstable, assembling and disassembling at successive positions around the cell surface [5, 7, 9, 11-13]. Motivated by the observation that faint and unstable domains are associated with slow surface growth [7, 9, 12], we sought to dissect the causal-effect relationships between growth and polarity, and assay in a systematic manner the impact of modulating surface growth rate on polarity stability.

Using the rod-shape fission yeast *Schizosaccharomyces pombe*, as an established model for polar growth [14], we first manipulated growth rate by reducing turgor pressure that serves as a physical driver for growth in walled cells [15]. We used a *gpd1Δ* mutant, defective in turgor adaptation, expressing the CRIB-3GFP probe to label active GTP-Cdc42, and used a defined concentration of sorbitol to reduce turgor and consequent growth rates in a reproducible manner [6, 16, 17]. In normal medium, *gpd1Δ* cells exhibited the same amount of tip-associated active-Cdc42 as WT, and no gross defect in cell shape, size and growth (Figure S1A). Using microfluidic flow chambers [18], we rapidly rinsed cells with medium containing 0.5 M sorbitol. This caused a transient cell shrinkage, followed by a stable reduction in growth rate of ~ 80% within 5-10 min (Figure 1A) [6]. Strikingly, as growth rate dropped, GTP-Cdc42 domains became dimmer and more spread with the appearance of transient ectopic patches of activity on cell sides (Figure 1A-1B; Movie S1). Both growth and polarity changes remained stable for at least one hour after treatment. CRIB-3GFP polarization index (PI), computed as the ratio of membrane-associated signal at cell tips to that of the whole cell contour, decreased from a mean value of 2.02 before treatment down to 1.50 after treatment. Importantly, rinsing cells back into normal medium led to a rapid raise in growth rate and concomitant increase in CRIB PI, suggesting this effect is reversible (Figure S1B). Similar treatment in WT cells, only yielded a partial and transient reduction of both growth rate and CRIB PI (Figure S1C).

As another means to affect growth, we abruptly reduced glucose content of yeast medium to 0.03%. This caused WT cells to swell transiently and was followed by a marked growth rate decrease (Figure 1C; Movie S1). CRIB PI also dropped following growth arrest, with cells

featuring cap spreading and occasional domains forming on cell sides (Figure 1C). Finally, we exploited a global slow growth phenotype of a *trk1Δtrk2Δ* mutant deficient in potassium import/export, which can be rescued by addition of 50 mM KCl to the medium [19]. We found that addition of KCl to these mutant cells increased their growth rate by ~30% within few minutes and was accompanied by a significant improvement in CRIB polarization (Figure S1D; Movie S1). Together, those results suggest that growth may positively influence the stability of active Cdc42 polarity domains.

Influence of growth on other polarity factors.

We next addressed the response of other polarisome components to turgor-reduction mediated growth arrest. Landmark factors such as microtubules and tea1-3GFP did not exhibit significant changes in their spatial distribution (Figure S1E and S1F). In contrast, polarity factors downstream of Cdc42 including the actin-associated protein bud6-3GFP, the type V myosin, myo52-3GFP, and exocyst components such as sec8-GFP, and sec6-GFP all showed some degree of reduced polarization with occasional domain assembly on cell sides, co-localized with CRIB (Figure 1D and S1F-G).

F-actin visualized with a GFP-LifeAct probe [20] remained mostly intact, suggesting that polarity defects were not caused by some indirect stress effects on actin polymerization. However, we noted some defects in the spatial organization of F-actin structures. At a short-time scale after sorbitol addition, endocytic patches exhibited a transient increase in number (Figure S1H) [21] . On longer time-scales of more than 5-10 min, the actin network appeared disorganized as compared to controls, with the occurrence of cable elongation and endocytic patches at cell sides, consistent with the presence of GTP-Cdc42 there (Figure 1D and S1H).

Finally, polarized integral membrane components transported in vesicles to cell tips, such as the cell wall synthase GFP-bgs4 and the SNARE GFP-syb1 exhibited near-complete detachment from the membrane with consequent enrichment in internal compartments (Figure 1D, S1F and S1I-J). Importantly, this complete detachment was not observed for non-polar integral membrane proteins such as GFP-psy1 [22], suggesting this response was not the result of potential pleiotropic insults on membrane shape and structure (Figure S1E-F). Those findings suggest that growth may positively influence the stability of Cdc42-based polarity as a whole.

Although growth reduction did not grossly affect actin polymerization, its impact on polarity was somewhat reminiscent of cells treated with the actin-depolymerizing drug latrunculin A (LatA) [23]. As LatA halts growth in yeast, we asked whether its effect on growth could account for some of its impact on polarity stability. Time-controlled LatA addition yielded a gradual decrease of the growth rate, eventually dropping to similar levels as with sorbitol treatment after 45 min (Figure 1E; Movie S1). Interestingly, CRIB polarization dropped with similar kinetics, but LatA caused CRIB domains to completely detach from cell tips and to reform on cell sides, as previously reported (Figure 1E) [23, 24].

We reasoned that F-actin could promote some of the remnant CRIB localization at cell tips in turgor-reduced cells, by mediating directly or indirectly GTP-Cdc42 domain association with tip landmarks such as tea1p. To test this, we arrested growth with sorbitol in a *gpd1Δ tea1Δ* double mutant. This led to a near complete depolarization, which recapitulated the effect of LatA treatment on CRIB domains in turgid cells (Figure 1F; Movie S1). Those results suggest that landmarks retain a fraction of active-Cdc42 at cell tips upon growth arrest, in an actin-dependent manner.

Finally, by computing the dependence of CRIB PI changes on growth rate variations using all aforementioned assays, we found a significant correlation ($r = 0.7604$) (Figure 1G). We conclude that growth may promote polarity stability in a dose-dependent manner.

Growth inhibition by physical confinement destabilizes polarity

Growth in turgid cells may be influenced by external mechanical barriers such as neighboring cells, physical obstacles or cell-encasing layers [6, 9, 13, 25]. To assay this, we designed dedicated narrow channels to confine cells laterally but allow them to grow from their ends [26, 27] (Figure 2A). WT cells growing in those channels initially proliferated with similar rates as controls outside (Figure S2A); but as density increased, they started to hamper one another's growth. Cells reaching high levels of confinement ceased growth or grew very slowly, and adopted small triangular or rectangular shapes (Figure 2B). Remarkably, growth-arrested cells exhibited weak CRIB domains oftentimes dynamically exploring the cell contour away from cell tips, reminiscent of turgor reduction assays (Figure 2B; Movie S2). Polar components, including bud6-3GFP, LifeAct-mCherry, sec6-GFP, sec8-GFP and GFP-bgs4, were also spatially destabilized as in turgor-reduction mediated growth arrest and exhibited dynamic changes of localization (Figure 2C-2D and S2D). Importantly, dynamic

assembly and disassembly of ectopic domains, was still highly pronounced in *mal3Δ* and *tea1Δ* mutants in channels, ruling out a role for microtubule-based polarity reorganization following shape changes, in CRIB domain instability (Figure S2B-C) [28, 29]. Thus, hampering growth by external mechanical means, can yield significant destabilization of polarity domains.

Because confinement in channels is reached as a result of multiple phases of growth and division; we devised an assay to rapidly suppress confinement and assay polarity response. We started with fully confined and depolarized cells and used UV-laser ablation to kill a subset of cells in the microchannel (Figure 2E; Movie S3) [9]. Ablated cells deflated within seconds, freeing space for adjacent cells to grow (Figure 2E). Strikingly, ~10 - 20 min after ablation, neighboring cells resumed rapid growth with the concomitant formation of bright and stable CRIB-3GFP domains at growth sites. Importantly, this response was also observed in cells at a further distance from the gaps, ruling out putative effects of chemical release from ablated cells or contact-inhibition cues on polarity stability (Figure 2E). Those findings demonstrate that cells can dynamically adapt their polarity behavior to different confinement states altering growth.

A candidate screen identifies suppressors and enhancers for the impact of growth on polarity stability

To identify potential factors mediating those effects, we then designed a candidate screen using the *gpd1Δ*-sorbitol growth arrest assay (Figure 3A). We selected candidates from different classes of sensing and regulating systems, including components of the cell wall integrity pathway, factors feeding into polarity and a set of globally acting protein kinases and modulators that have been implicated in growth or polarity before (Figure 3B and S3A-D). We crossed candidate mutants into a *gpd1Δ* background expressing CRIB-3GFP or CRIB-3Citrine [24], and computed the ratio of CRIB PI after and before sorbitol addition (Figure S3A-S3D). This screen identified suppressors, in which CRIB PI after growth reduction was maintained at a higher level than *gpd1Δ* controls. Mutants in actin cable-dependent transport, like a mutant in the formin for3, and in the myosin typeV, myo52 had the most pronounced suppressing effect [14]. Mutants in signaling components including the stress-related MAP Kinase sty1 and in the TOR-activating Rab-family GTPase ryh1, exhibited a lower, yet significant suppression (Figure 3B-D and S3D) [30, 31] . This

screen also identified enhancers including mutants for the Cdc42 GAP rga4 and in the landmark tea1, as discussed above (Figure 1F and Figure 3B). As both factors have established roles in confining GTP-Cdc42 to cell tips; this result could reflect that spatial landmarks outcompete the basal destabilizing impact of growth arrest on polarity. Finally, a mutant in the endocytosis-promoting factor end4 and in the Cdc42 GEF gef1 also exhibited milder enhancing effects (Figure 3B-D).

To test the epistatic relationships between suppressing pathways, we compared the responses of *gpd1Δfor3Δ*, *gpd1Δsty1Δ* and *for3Δsty1Δ* with *gpd1Δ* alone (Figure 3E-3F and S3E). We resorted to using the *for3Δsty1Δ* mutant, as we were unable to obtain a viable *gpd1Δfor3Δsty1Δ* triple mutant, but noted that this double mutant, as in *gpd1Δ* background strains, did not adapt growth upon sorbitol treatment, due to the absence of sty1. Interestingly, in *for3Δsty1Δ* cells we found that polarization upon growth arrest remained nearly indistinguishable from the pre-treatment state (Figure 3E and F). Although this analysis, cannot fully rule out unknown direct effects of gpd1 on polarity stability, it indicates that actin cable-mediated transport acts independently of sty1 in this response.

As sty1p is an established downstream target of hyperosmotic treatments, and can drive active-Cdc42 dispersal from cell tips when ectopically activated [24] the suppressing effects of *sty1Δ* could represent an assay-specific bias. However, the effect on polarity removal here is rather mild as compared to that reported for ectopic activation. Thus, an open possibility is that sty1 becomes partly activated as a general response to growth arrest and contributes to the detachment of GTP-Cdc42. The implication of actin-based vesicle delivery, which feeds directly into Cdc42 polarity, may be more generic, and suggests that an imbalance or a mis-regulation of vesicles fluxes could serve as a core mechanism allowing cells to adapt polarity to their growth rate [5, 8]. Vesicle flows into the tip membrane may have enhanced polarity diluting effects when surface growth is slowed down [8, 32, 33]. An alternative effect could come from defects in vesicle docking and/or fusion associated with alterations in tip membrane biochemistry or mechanics, resulting from growth defects.

One interesting finding is that endocytosis appears to promote the maintenance of active-Cdc42 at cell tips but is required for the detachment of the cell wall synthase bgs4 from cell tips (Figure S1J). Accordingly, the detachment of bgs4 happens much slower, and was recently reported to depend on the cell wall mechanical sensor wsc1 [34], which did not

appear to affect active-Cdc42 detachment (Figure 3B). This suggests that different mechanisms acting at various time-scales may control the response of polarity and growth-promoting components to growth arrest.

Feedbacks between growth and polarity as means to reorient growth around physical obstacles.

We then asked what could be the functional relevance of a feedback between growth and polarity stability. By observing cells growing in 1D or 2D microchannels, we noted that cell tips that met end-on and were unable to displace one another, systematically started to grow into available spaces by actively reorienting polar growth, yielding a high proportion of bent cells (Figure 4A and 4B). Such behavior implicated a first phase of destabilized polarity due to growth blockage by other cells, which served to locate empty spaces. This was evident from monitoring cells that grew onto each other or onto an obstacle, like a non-germinated spore (Figure 4C and S4A; Movie S4). In those instances, polarity could dynamically reorient multiple times, sometimes stabilizing at the other cell end, before causing marked shape changes, in a window as short as 20-30 min responding to newly available narrow gaps (Figure 4C, 40').

Furthermore, we observed a similar dynamic behavior outside a microchannel using an *ace2Δ* mutant, in which cell separation is strongly impaired. This mutant bears defects in cell separation, yielding chains of 4 or more cells, with flanked middle cells that cannot grow from their tips [35]. In middle cells, CRIB-3GFP domains were weak and dynamically changed their positions and became bright and stable upon outgrowth from the side of the chain, much like WT cells in channels (Figure 4D). This behavior was never observed in front cells free to grow from their tips. We conclude that a positive feedback between growth and polarity provides cells with a functional module to dynamically reorient their growth axis towards empty spaces.

Universality of feedbacks between growth and polarity

To test if this effect was a conserved feature of tip growing cells, we assayed responses in several filamentous fungus species belonging to distant branches of the fungal tree including zygomycetes (*Mucor*), basidiomycetes (*Trametes and Coprinus*) and ascomycetes (*Sordaria*

and *Botrytis*) (Figure S4B). We grew fungi in flow channels, rinsed them in hyperosmotic medium (0.2 - 0.5 M sorbitol, depending on the species) and monitored their directional response after osmo-adaptation. This treatment led to a complete cessation of hyphal growth, followed by a resumption of rapid growth after an adaptation delay (Figure 4E and S4C). Strikingly, when cell growth recommenced, hyphae frequently grew from the sides of the apex in 50-70% of cases and occasionally branched (Figure 4F-4G). This response was independent of hyphal diameter and also prominent in newly formed branches. Importantly, this altered polarized behavior was dependent on growth arrest, as flowing in medium did not affect hyphal polarization (Figure 4G and Figure S4D). In some species, like *Botrytis* or *Mucor*, lateral branch formation following growth arrest, was preceded by a brief period of isotropic growth, indicative of initial polarity dispersal before local stabilization (Figure 4F and H). One species, *Coprinus cinereus*, formed lateral branches following growth arrest and recovery, mainly at large distances from the apex (30-60 µm), plausibly reflecting inherent mechanisms that suppress tip-proximal branching (Figure S4E). Although this growth redirection behavior created some sharp shape changes at the hyphal tip, we noted that, on a global scale, hyphae continued their mean growth direction away from the bulk of the colony, likely guided by some tropisms [1]. Those results support a plausible universality for a feedback between growth and polarity relevant to most fungal species.

In sum, we propose a dynamic feedback linking growth and polarity stability: when polarity domains form at the surface, they become stable if growth occurs at a normal/high rate; and disassemble if growth is hindered mechanically or chemically (Figure S4F). This feedback may account for persistent polar growth typical of yeast and fungal cells independently of guiding cues or spatial landmarks [9, 36, 37]. Accordingly, this mechanism appears more prominent in the absence of internal landmarks provided by the tea1 system in fission yeast and may compete with global guiding cues in fungal hyphae (Figure 1F and 4F). This feedback could also synchronize, or phase-lock, Rho GTPases oscillations and pulsatile growth typical of many tip-growing cells [38, 39]. One important realization however is that growth rates in yeast and other walled cells remain bounded. Thus, in addition to positive feedbacks, limitation systems either based upon the availability of polarity/growth factors or encoded in the mechanics of the surface must exist to buffer growth [34].

In addition to conferring spatial persistency to polar growth, this mechanism also provides flexibility, by allowing cells to reorient growth in directions, which are mechanically favorable. Many tip growing cells, including fungal hyphae and plant roots, exhibit

thigmotropisms and can redirect their growth axis in response to mechanical stimuli, when navigating in tissues or in soil, for instance [40]. The feedback we document here, could in principle serve as an inherited trait promoting such behavior even in a simple yeast cell.

While growth is the prominent driver of cell surface deformation in fungal cells, other eukaryotic cells which migrate or are submitted to tissue forces may also employ similar conceptual feedbacks to support the stability of polarity machineries with respect to their rates of surface deformation. Accordingly, recent work has suggested near-universal correlations between directional persistence and locomotion speed in migrating cells [41]. Cell surface deformations, which originate form patterns of tissue stress may also promote cell polarization along specific tissue axis in animal [42] and plant tissues [43]. Further work addressing the interconnections between dynamic shape changes and directional behaviors shall enlighten mechanisms of eukaryotic morphogenesis.

ACKNOWLEDGMENTS

The authors acknowledge M. Balasubramanian, Q. Chen, M. Edamatsu, S. Martin, P. Perez, Y. Sanchez, K. Sawin and F. Leclerc for sharing strains and material. This work was supported by the CNRS and grants from the FP7 CIG program (no. 303821), the Mairie de Paris “Emergence” program, and the European Research Council (CoG Forcaster n° 647073).

AUTHOR CONTRIBUTIONS

A.H. performed experiments and analyzed data. D.E. developed image analysis scripts. A.H. and N.M. designed the research and wrote the manuscript.

DECLARATON OF INTERESTS

The authors declare that they have no competing interests.

REFERENCES:

1. Brand, A., and Gow, N.A. (2009). Mechanisms of hypha orientation of fungi. Curr Opin Microbiol *12*, 350-357.
2. Merlini, L., Dudin, O., and Martin, S.G. (2013). Mate and fuse: how yeast cells do it. Open Biol *3*, 130008.
3. Li, R., and Gundersen, G.G. (2008). Beyond polymer polarity: how the cytoskeleton builds a polarized cell. Nat Rev Mol Cell Biol *9*, 860-873.
4. Johnson, J.M., Jin, M., and Lew, D.J. (2011). Symmetry breaking and the establishment of cell polarity in budding yeast. Curr Opin Genet Dev *21*, 740-746.
5. Martin, S.G. (2015). Spontaneous cell polarization: Feedback control of Cdc42 GTPase breaks cellular symmetry. Bioessays *37*, 1193-1201.
6. Minc, N., Boudaoud, A., and Chang, F. (2009). Mechanical forces of fission yeast growth. Curr Biol *19*, 1096-1101.
7. Bendezu, F.O., and Martin, S.G. (2013). Cdc42 explores the cell periphery for mate selection in fission yeast. Curr Biol *23*, 42-47.
8. Bonazzi, D., Haupt, A., Tanimoto, H., Delacour, D., Salort, D., and Minc, N. (2015). Actin-Based Transport Adapts Polarity Domain Size to Local Cellular Curvature. Curr Biol *25*, 2677-2683.
9. Bonazzi, D., Julien, J.D., Romao, M., Seddiki, R., Piel, M., Boudaoud, A., and Minc, N. (2014). Symmetry Breaking in Spore Germination Relies on an Interplay between Polar Cap Stability and Spore Wall Mechanics. Dev Cell *28*, 534-546.
10. Merlini, L., Khalili, B., Bendezu, F.O., Hurwitz, D., Vincenzetti, V., Vavylonis, D., and Martin, S.G. (2016). Local Pheromone Release from Dynamic Polarity Sites Underlies Cell-Cell Pairing during Yeast Mating. Curr Biol *26*, 1117-1125.
11. Dyer, J.M., Savage, N.S., Jin, M., Zyla, T.R., Elston, T.C., and Lew, D.J. (2013). Tracking shallow chemical gradients by actin-driven wandering of the polarization site. Curr Biol *23*, 32-41.
12. Howell, A.S., Jin, M., Wu, C.F., Zyla, T.R., Elston, T.C., and Lew, D.J. (2012). Negative feedback enhances robustness in the yeast polarity establishment circuit. Cell *149*, 322-333.
13. Thomson, D.D., Wehmeier, S., Byfield, F.J., Janmey, P.A., Caballero-Lima, D., Crossley, A., and Brand, A.C. (2015). Contact-induced apical asymmetry drives the thigmotropic responses of Candida albicans hyphae. Cell Microbiol *17*, 342-354.
14. Chang, F., and Martin, S.G. (2009). Shaping fission yeast with microtubules. Cold Spring Harb Perspect Biol *1*, a001347.
15. Davi, V., and Minc, N. (2015). Mechanics and morphogenesis of fission yeast cells. Curr Opin Microbiol *28*, 36-45.
16. Ohmiya, R., Yamada, H., Nakashima, K., Aiba, H., and Mizuno, T. (1995). Osmoregulation of fission yeast: cloning of two distinct genes encoding glycerol-3-phosphate dehydrogenase, one of which is responsible for osmotolerance for growth. Mol Microbiol *18*, 963-973.
17. Tatebe, H., Nakano, K., Maximo, R., and Shiozaki, K. (2008). Pom1 DYRK regulates localization of the Rga4 GAP to ensure bipolar activation of Cdc42 in fission yeast. Curr Biol *18*, 322-330.
18. Charvin, G., Cross, F.R., and Siggia, E.D. (2008). A microfluidic device for temporally controlled gene expression and long-term fluorescent imaging in unperturbed dividing yeast cells. PLoS One *3*, e1468.
19. Calero, F., Gomez, N., Arino, J., and Ramos, J. (2000). Trk1 and Trk2 define the major K(+) transport system in fission yeast. J Bacteriol *182*, 394-399.
20. Courtemanche, N., Pollard, T.D., and Chen, Q. (2016). Avoiding artefacts when counting polymerized actin in live cells with LifeAct fused to fluorescent proteins. Nat Cell Biol *18*, 676-683.
21. Basu, R., Munteanu, E.L., and Chang, F. (2014). Role of turgor pressure in endocytosis in fission yeast. Mol Biol Cell *25*, 679-687.

22. Nakamura, T., Nakamura-Kubo, M., Hirata, A., and Shimoda, C. (2001). The Schizosaccharomyces pombe spo3+ gene is required for assembly of the forespore membrane and genetically interacts with psy1(+)-encoding syntaxin-like protein. Mol Biol Cell *12*, 3955-3972.
23. Bendezu, F.O., and Martin, S.G. (2011). Actin cables and the exocyst form two independent morphogenesis pathways in the fission yeast. Mol Biol Cell *22*, 44-53.
24. Mutavchiev, D.R., Leda, M., and Sawin, K.E. (2016). Remodeling of the Fission Yeast Cdc42 Cell-Polarity Module via the Sty1 p38 Stress-Activated Protein Kinase Pathway. Curr Biol *26*, 2921-2928.
25. Sampathkumar, A., Yan, A., Krupinski, P., and Meyerowitz, E.M. (2014). Physical forces regulate plant development and morphogenesis. Curr Biol *24*, R475-483.
26. Goulev, Y., Morlot, S., Matifas, A., Huang, B., Molin, M., Toledano, M.B., and Charvin, G. (2017). Nonlinear feedback drives homeostatic plasticity in H2O2 stress response. Elife *6*.
27. Zegman, Y., Bonazzi, D., and Minc, N. (2015). Measurement and manipulation of cell size parameters in fission yeast. Methods Cell Biol *125*, 423-436.
28. Minc, N., Bratman, S.V., Basu, R., and Chang, F. (2009). Establishing new sites of polarization by microtubules. Curr Biol *19*, 83-94.
29. Terenna, C.R., Makushok, T., Velve-Casquillas, G., Baigl, D., Chen, Y., Bornens, M., Paoletti, A., Piel, M., and Tran, P.T. (2008). Physical mechanisms redirecting cell polarity and cell shape in fission yeast. Curr Biol *18*, 1748-1753.
30. Millar, J.B., Buck, V., and Wilkinson, M.G. (1995). Pyp1 and Pyp2 PTPases dephosphorylate an osmosensing MAP kinase controlling cell size at division in fission yeast. Genes Dev *9*, 2117-2130.
31. Tatebe, H., Morigasaki, S., Murayama, S., Zeng, C.T., and Shiozaki, K. (2010). Rab-family GTPase regulates TOR complex 2 signaling in fission yeast. Curr Biol *20*, 1975-1982.
32. Savage, N.S., Layton, A.T., and Lew, D.J. (2012). Mechanistic mathematical model of polarity in yeast. Mol Biol Cell *23*, 1998-2013.
33. Tay, Y.D., Leda, M., Spanos, C., Rappsilber, J., Goryachev, A., and Sawin, K. (2018). Fission yeast NDR/LATS kinase Orb6 regulates exocytosis via phosphorylation of exocyst complex. bioRxiv.
34. Davì, V., Tanimoto, H., Ershov, D., Haupt, A., De Belly, H., Le Borgne, R., Couturier, E., Boudaoud, A., and Minc, N. (2018). Mechanosensation Dynamically Coordinates Polar Growth and Cell Wall Assembly to Promote Cell Survival. Developmental Cell *45*, 170-182.e177.
35. Dekker, N., Speijer, D., Grun, C.H., van den Berg, M., de Haan, A., and Hochstenbach, F. (2004). Role of the alpha-glucanase Agn1p in fission-yeast cell separation. Mol Biol Cell *15*, 3903-3914.
36. Kelly, F.D., and Nurse, P. (2011). De novo growth zone formation from fission yeast spheroplasts. PLoS One *6*, e27977.
37. Sawin, K.E., and Snaith, H.A. (2004). Role of microtubules and tea1p in establishment and maintenance of fission yeast cell polarity. J Cell Sci *117*, 689-700.
38. Das, M., Drake, T., Wiley, D.J., Buchwald, P., Vavylonis, D., and Verde, F. (2012). Oscillatory dynamics of Cdc42 GTPase in the control of polarized growth. Science *337*, 239-243.
39. Hwang, J.U., Gu, Y., Lee, Y.J., and Yang, Z. (2005). Oscillatory ROP GTPase activation leads the oscillatory polarized growth of pollen tubes. Mol Biol Cell *16*, 5385-5399.
40. Jaffe, M.J., Leopold, A.C., and Staples, R.C. (2002). Thigmo responses in plants and fungi. Am J Bot *89*, 375-382.
41. Maiuri, P., Rupprecht, J.F., Wieser, S., Ruprecht, V., Benichou, O., Carpi, N., Coppey, M., De Beco, S., Gov, N., Heisenberg, C.P., et al. (2015). Actin flows mediate a universal coupling between cell speed and cell persistence. Cell *161*, 374-386.
42. Aw, W.Y., Heck, B.W., Joyce, B., and Devenport, D. (2016). Transient Tissue-Scale Deformation Coordinates Alignment of Planar Cell Polarity Junctions in the Mammalian Skin. Curr Biol *26*, 2090-2100.

43. Nakayama, N., Smith, R.S., Mandel, T., Robinson, S., Kimura, S., Boudaoud, A., and Kuhlemeier, C. (2012). Mechanical regulation of auxin-mediated growth. Curr Biol *22*, 1468-1476.
44. Sato, M., Dhut, S., and Toda, T. (2005). New drug-resistant cassettes for gene disruption and epitope tagging in Schizosaccharomyces pombe. Yeast *22*, 583-591.
45. Fehrmann, S., Paoletti, C., Goulev, Y., Ungureanu, A., Aguilaniu, H., and Charvin, G. (2013). Aging yeast cells undergo a sharp entry into senescence unrelated to the loss of mitochondrial membrane potential. Cell Rep *5*, 1589-1599.
46. Bendezu, F.O., Vincenzetti, V., Vavylonis, D., Wyss, R., Vogel, H., and Martin, S.G. (2015). Spontaneous Cdc42 polarization independent of GDI-mediated extraction and actin-based trafficking. PLoS Biol *13*, e1002097.

FIGURE LEGENDS

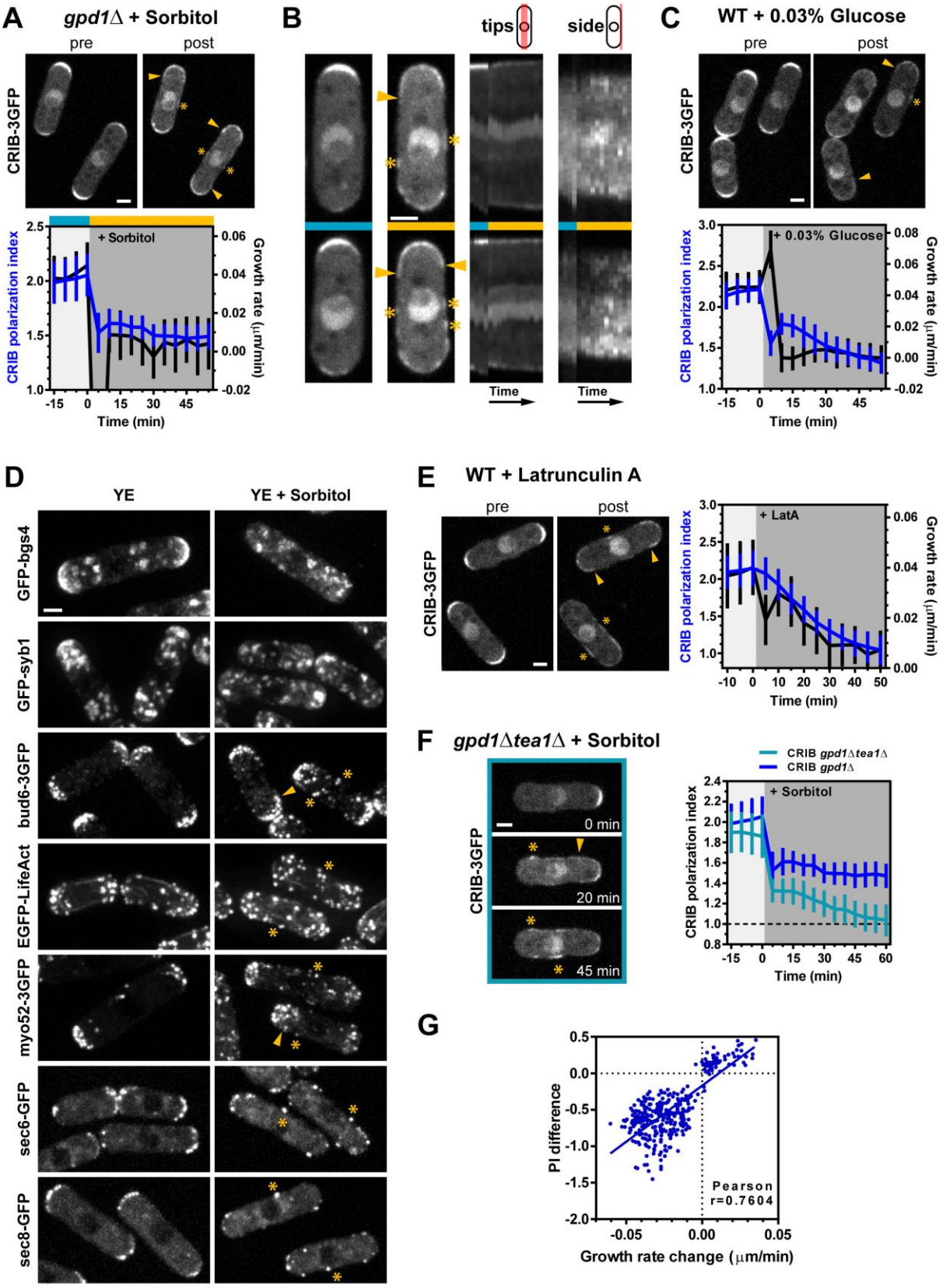

Figure 1 (Related to Figure S1 and Movie S1): Abrupt growth rate changes alter the localization of cell polarity factors.

A) *gpd1Δ* cells expressing CRIB-3GFP rinsed in YE medium with 0.5 M sorbitol to reduce turgor pressure and halt growth (n=36). Top: Representative cells before and after treatment. Bottom: Evolution of growth rate (black) and CRIB-3GFP polarization index (PI, blue). B) Representative *gpd1Δ* CRIB-3GFP cells before (left) and after (right) sorbitol treatment. Right: Kymographs of the same cells as in left panels showing signal intensities of a central 1.6 µm and a lateral 0.5 µm segments over 80 min with 5 min intervals. Colors correspond to growth conditions as labeled in the graph in A. C) Wild type cells expressing CRIB-3GFP rinsed in YE medium with 0.03% Glucose (n=46). Top: Representative cells before and after treatment. Bottom: Evolution of growth rate (black) and CRIB-3GFP polarization index (PI, blue). D) Subcellular localization patterns of different polarity factors in *gpd1Δ* cells in YE and after 30 min of treatment in YE + 0.5 M sorbitol. E) Wild type cells expressing CRIB-3GFP treated with 50 µM Latrunculin A (LatA) (n=46). Left: Representative cells before and after treatment. Right: Evolution of growth rate (black) and CRIB-3GFP polarization index (PI, blue). F) *gpd1Δ* (n=36) and *gpd1Δ tea1Δ* (n=45) cells treated with 0.5 M sorbitol. Left: Changes in CRIB-3GFP localization in *gpd1Δtea1Δ* cells. Right: Evolution of PI over time for both strains. G) Correlation of CRIB-3GFP PI changes as a function of growth rate changes of all cells from experiments in A, C, E and F. Pearson correlation coefficient, r=0.7604. In all images arrowheads label spread caps and asterisks mark lateral accumulations of polarity factors. Scale bars, 2 µm. Error bars represent standard deviations. Data are from two or more independent experiments.

436

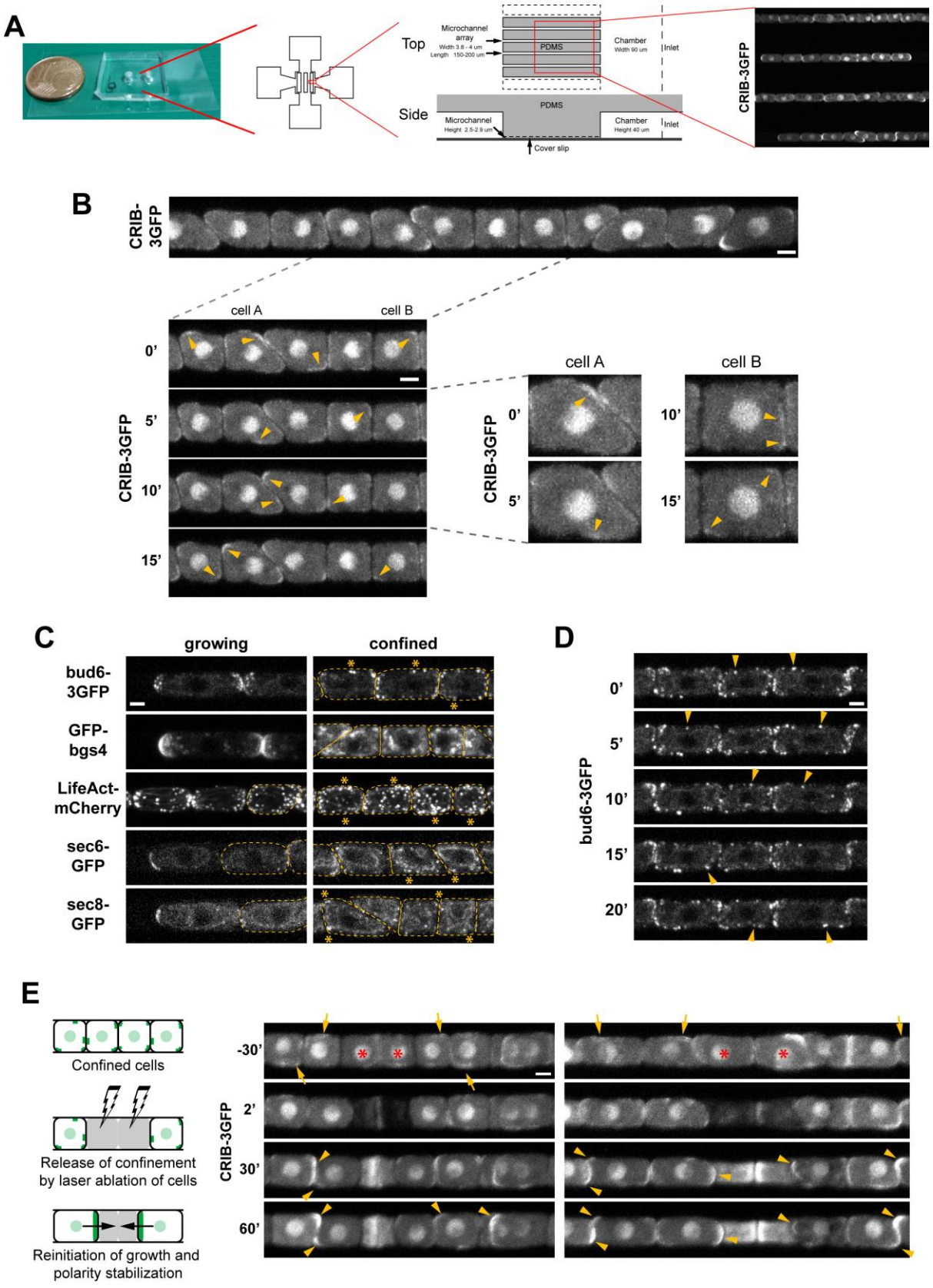
A
Top
Microchannel array
Width 3.8 - 4 um
Length 150-200 um
PDMS
Chamber
Width 90 um
Inlet
Side
Microchannel
Height 2.5-2.9 um
PDMS
Chamber
Height 40 um
Inlet
Cover slip
CRIB-3GFP
B
CRIB-3GFP
cell A
cell B
0'
5'
10'
15'
CRIB-3GFP
cell A
cell B
0'
5'
10'
15'
C
growing
confined
bud6-3GFP
GFP-bgs4
LifeAct-mCherry
sec6-GFP
sec8-GFP
D
bud6-3GFP
0'
5'
10'
15'
20'
E
Confined cells
Release of confinement by laser ablation of cells
Reinitiation of growth and polarity stabilization
CRIB-3GFP
-30'
2'
30'
60'

437

Figure 2 (Related to Figure S2 and Movie S2 and S3): Growth arrest through mechanical confinement triggers polarity domain destabilization and wandering.

A) Large-scale picture and schematic representation of microchannel design. Three columns, each containing microchannel arrays of different length, are embedded within a large medium reservoir ('chamber') for optimal nutrient supply. B) WT cells expressing CRIB-3GFP grown to confinement in microchannels (top). Arrowheads label transiently forming CRIB domains on the surface. Time-lapse of confined cells (bottom left) and close-up view of two cells as labeled on the left (bottom right). C) WT cells expressing the indicated polarity markers grown in free-growing and fully confined regions in the same set of microchannels. D) WT cells expressing bud6-3GFP grown to full confinement in microchannels. Arrowheads label transiently forming bud6-3GFP ectopic small domains wandering on the surface. E) Wild type cells expressing CRIB-3GFP were grown in microchannels to full confinement and two cells, labelled with red asterisks, were ablated with a UV-laser to free space for neighbors to grow. Arrows label initially transient or weak CRIB domains and arrowheads depict reforming stable CRIB domains. Scale bars, 2 μm.

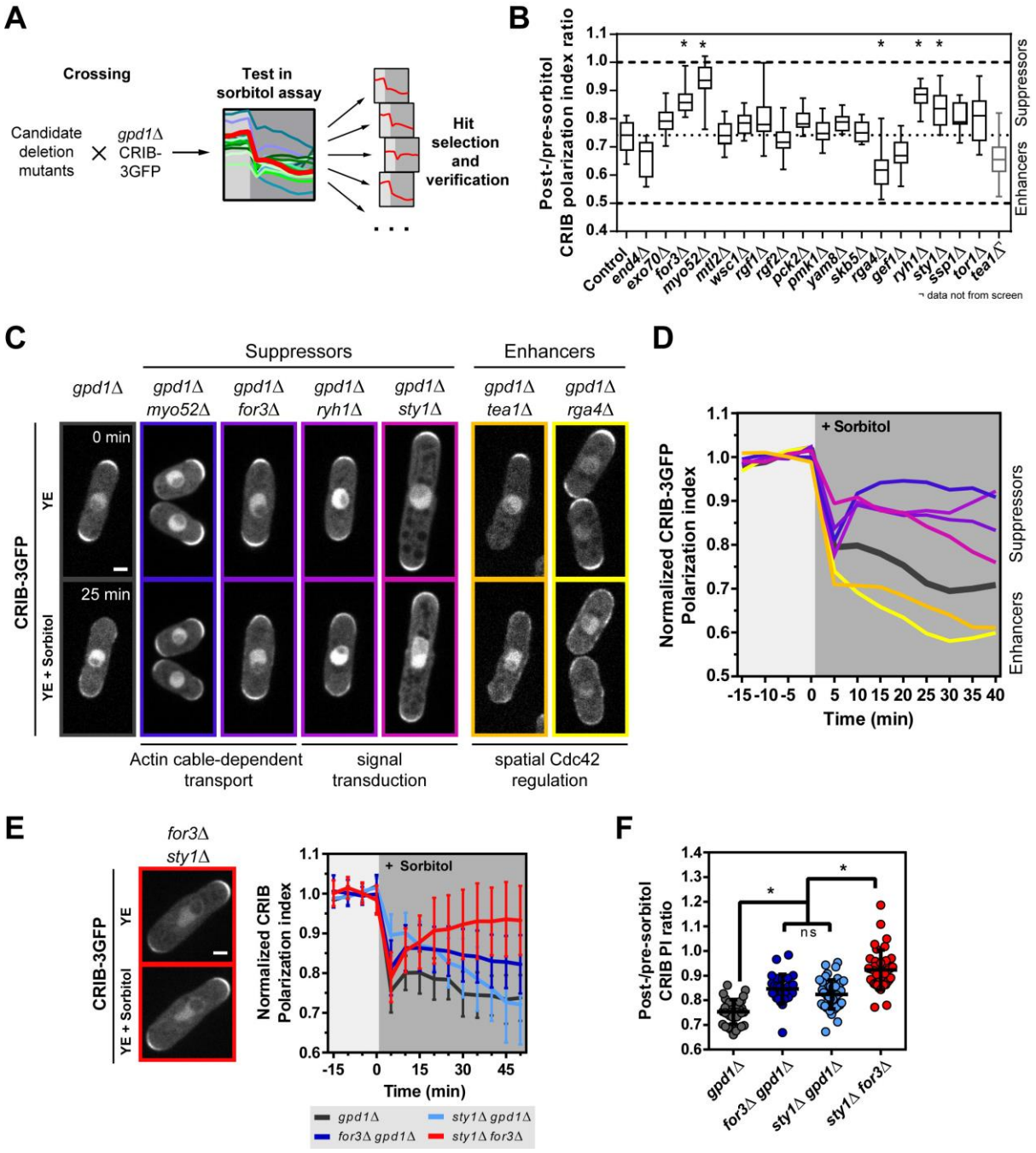

Figure 3 (Related to Figure S3): Candidate genetic screen for modulators of active-Cdc42 domain destabilization upon growth reduction.

A) Schematic representation of the screening approach. B) Overview of screen results plotted as post/pre-sorbitol ratio of CRIB-3GFP polarization index. Box plots depict the mean with 25th and 75th percentiles and whiskers the full data range. Dotted lines indicate upper and lower limits of the range of values for no change or complete loss of polarization, respectively. The middle dotted line depicts values for the control. For control vs. *for3Δ*, *myo52Δ*, *ryh1Δ*, *rga4Δ*, and *sty1Δ*, there was a statistically significant difference between groups as determined by one-way ANOVA ($F(19, 330) = 40.49$, $p < 0.0001$). *tea1Δ* values

plotted for comparison are derived from experiment in Figure 1F but were not included in the statistical analysis because of non-matching experimental conditions. C) Representative images of CRIB-3GFP response of candidates derived from the screen directly before (0 min) and 25 min after exposure to 0.5 M sorbitol. D) Mean response curves of CRIB-3GFP PI for hits from the screen. Colors and genotypes are matched with panel C. E) Effect of *for3Δ* and *sty1Δ* deletions on CRIB-3GFP polarization upon treatment with 0.5 M sorbitol. Left: Image shows CRIB-3GFP distribution in *for3Δ sty1Δ* cells before and after sorbitol treatment. Right: CRIB-3GFP PI during sorbitol treatment (*gpd1Δ* (n=36), *for3Δ gpd1Δ* (n=28), *sty1Δ gpd1Δ* (n=34) and *for3Δ sty1Δ* (n=39)). F) Comparison of post/pre-sorbitol PI ratio of CRIB-3GFP.. For *gpd1Δ*, *for3Δ gpd1Δ*, *sty1Δ gpd1Δ*, and *for3Δ sty1Δ*, there was a statistically significant difference between groups as determined by one-way ANOVA ($F(3, 144) = 45.112$, $p < 0.0001$). Scale bars, 2 μm. Error bars represent standard deviations. Data, except in B, come from two or more independent experiments.

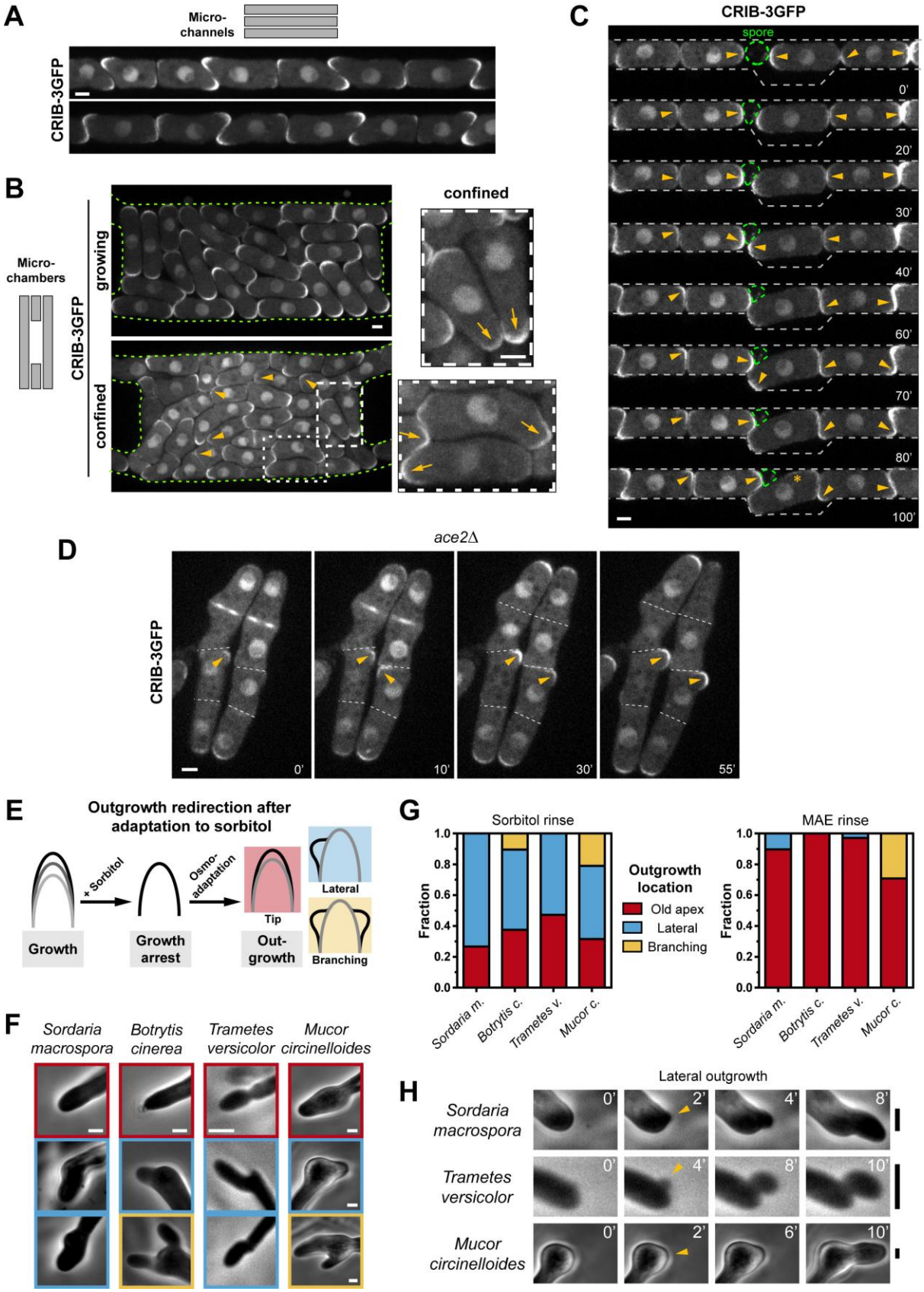

Figure 4 (Related to Figure S4 and Movie S4): Universal feedback between growth and polarity as a means to reorient polar growth axis.

A) Wild type cells expressing CRIB-3GFP grown in microchannels and observed at a stage of early confinement. B) Wild type cells expressing CRIB-3GFP grown in 2D microchambers and observed at a stage of low (left top) and high (left bottom) confinement. Insets show magnifications of cells in high confinement (right). Arrowheads point at examples of weak CRIB-3GFP domains and arrows label irregularly shaped cell tips. C) WT cells expressing CRIB-3GFP growing from the two opposite ends of a channel and reorienting polarity and growth upon contact. Arrowheads indicate CRIB domains that change position. The green dashed circle depicts the outline of a dormant spore acting as a rigid obstacle. D) *ace2Δ* cells expressing CRIB-3GFP grown on YE agar. As a consequence of delayed cell separation some cells are flanked by two sister cells and finally outgrow from the sides. Arrowheads label initially transient or weak CRIB domains that become stabilized and intense as cells outgrow. E) Assaying outgrowth direction of filamentous fungi after recovery from sorbitol-induced growth arrest. F) Representative hyphal shapes following growth recovery after sorbitol treatment in various fungal species. Colors are related to response classification in Figure 4G. G) Quantification of the different hyphal phenotypes reflecting a transient alteration of polarization behavior following growth arrest and recovery. For sorbitol rinse: *S.m.* n=30, *B.c.* n=39, *T.v.* n=36, *M.c.* n=19. For MAE rinse: *S.m.* n=29, *B.c.* n=26, *T.v.* n=34, *M.c.* n=24. H) Time-lapse of lateral outgrowth at the hyphal tips in different species. Scale bars, 2 μm (A-E) and 4 μm (F-H).

STAR METHODS:

CONTACT FOR REAGENT AND RESOURCE SHARING

Further information and requests for resources and reagents should be directed to and will be fulfilled by the lead contact, Nicolas Minc (nicolas.minc@ijm.fr).

EXPERIMENTAL MODEL AND SUBJECT DETAILS

Yeast strains, genetic methods, and media

Standard methods for *S. pombe* media and genetic manipulations were used (www-bcf.usc.edu/~forsburg; www.biotwiki.org/foswiki/bin/view/Pombe/NurseLabManual). Strains used in this study are listed in the key resource table. Marker switching from Kan to Nat was achieved by amplifying the NatMX cassette from a pCR2.1-nat vector with primers MD1 and MD2 and transforming it into KanMX cassette-bearing strains. Positive clones were selected on YE5S + 50 µg/ml Nat plates and tested for functional and visual phenotypes [44]. For all experiments, liquid cultures were grown in YE5S (containing 3% glucose) overnight at 25°C. For experiments in flow channels, cells were pre-stained with 10 µg/ml Alexa647-labeled isolectin GS-IB4 from *Griffonia simplicifolia* (Thermo Fisher Scientific, Waltham, Massachusetts, USA) and growth medium contained a constant Lectin supply of 5 µg/ml. The lectin signal labelled the cell contour and was used for cell segmentation during image analysis.

Filamentous fungi species, media and growth:

Strains: *Botrytis cinerea*, *Sordaria macrospora*, *Coprinus cinereus*, *Trametes versicolor* and *Mucor circinelloides*. All strains were grown on MAE medium (2% malt, 0.1% peptone, 2% glucose) either as liquid or plates with 2% agar. To grow hyphal mycelia, spores were prepared by lysing hyphae from a fully-grown MAE plate with glass beads and a FastPrep device (MP Biomedicals, Santa Ana, California, USA). Crude spore preparations were used to inoculate 20 ml MAE cultures and these were grown over night at 25°C. Emerging mycelia from these cultures were placed in PDMS flow channels under a dialysis membrane for microscopy.

Pharmacological inhibition

Latrunculin A (Sigma-Aldrich, St. Louis, Missouri, USA) was used at a final concentration of 50 µM from a 200x stock in DMSO (Euromedex, Souffelweyersheim, France). CK666 (Sigma-Aldrich) was used at a final concentration of 100 µM from a 500x stock in DMSO. DMSO amounts in control experiments were adjusted correspondingly for each drug.

METHOD DETAILS

Flow channels

We used two kinds of flow channels depending on the type of experiment. For drug treatments we used a simple glass channel built from one 24x50 mm (VWR, Radnor, Pennsylvania, USA) and a 22x22 mm (Thermo Fisher Scientific) coverslip spaced by ~ 250 µm, using double-sided adhesive tape. To make cells adhere to the glass surface, the flow channel was pre-coated with 1 mg/ml poly-L-lysine (Sigma-Aldrich) and 0.1 mg/mg isolectin GS-IB4 from *Griffonia simplicifolia*, (Thermo Fisher Scientific).

In the second type of flow channels, cells were placed beneath a single layer of dialysis membrane and covered with a polydimethylsiloxane (PDMS) channel, allowing for exchange of the medium [18].

Microchannels for confined growth assays

Design and fabrication

The general design of microchannels to confine fission yeast cells is shown in Figure 2A. Those channels were optimized to ensure a near unlimited nutrient supply, and implicated a 2-step soft-lithography microfabrication technique [45]. A first thin layer of ~2.5 µm in height was first fabricated using SU8 photoresists, and subsequent UV illumination through a Quartz mask. Subsequently, a second layer of ~40µm in height of SU8 photoresists, was spread on top of the first layer, and exposed with UV through a Quartz mask, aligned with the first design using a Mask Aligner . PolyDimethylSiloxane (PDMS, Sylgard 184 from Dow Corning, Midland, Michigan, USA) replica were prepared using a 10:1 ratio of PDMS:curing agent.

Microchannel assembly

PDMS channels were covalently mounted onto 24x50 mm cover slips (VWR) [27]. To this aim, coverslips were cleaned with Acetone, Isopropanol and ddH_2O. For covalent binding, both channel and coverslip were then plasma treated for 1 min, mounted and baked at 65°C for ≥ 1 h.

Cell loading and growing

Cell were loaded into channels as spores, which then germinated and proliferated as vegetative cells, crowding the channels [27] . Spores were obtained from *h90* strains sporulated on ME/3% agarose (Formedium, Hunstanton, UK)/(Sigma-Aldrich) plates at 25°C for 2-3 days. Mating mixtures were digested in 1/200 Glusulase (PerkinElmer, Waltham, Massachusetts, USA) at room temperature overnight, to eliminate vegetative cells. Digests were cleared of debris by adding four volumes of Percoll (Sigma-Aldrich), followed by a centrifugation at 600 rcf for 3min and supernatant removal. Spores were washed once with five volumes of YE5S and subsequently re-suspended in YE5S medium [46]. Channels were first filled with YE5S and subsequently a high density spore solution was pushed into channels with a syringe, usually yielding 1-6 spores per channel. Excess spores were rinsed out. Filled channels were incubated for 18-24 h in a humidified petri dish at 25 or 30°C, depending on global spore density after seeding. The next morning, channels were rinsed with fresh media at least 1h before live-imaging.

Microscopy

For immediate imaging, 1.8 µl of fresh, concentrated cells were placed between a glass slide and coverslip and imaged within 20 min. For experiments with dynamic exchange of growth media / drug addition, cells were placed in different types of flow channels. Microchannels were directly imaged.

All fission yeast imaging was carried out at room temperature (22–25°C) with an inverted spinning-disk confocal microscope equipped with a motorized stage and automatic focus (Ti-Eclipse, Nikon, Minato, Tokyo, Japan), a Yokogawa CSUX1FW spinning unit, and an EM-CCD camera (ImagEM-1K, Hamamatsu Photonics, Japan). Images were acquired with a 100× oil-immersion objective (CFI Plan Apo DM 100x/1.4 NA, Nikon). For laser ablation in microchannels we used an iLas2 module (Roper Scientific) with a 355 nm laser and acquired images with a 60x oil-immersion objective (CFI Apochromat 60x Oil λS, 1.4 NA, Nikon) in

combination with a 2.5x magnifying lens. The microscope was operated with Metamorph software (Molecular Devices).

Presented images represent single confocal slices or specific z-stacks: Figure 1A, 1E, 1F, 3C and 3E: Single-plane confocal images. Figure 1D: Maximum intensity projections of 19 z-slices spaced by 0.25 μm, except for sec8-GFP which is a projection of 3 slices spaced by 0.5 μm. Figure 2B: Maximum intensity projections from 5 z-slices spaced by 0.6 μm. Figure 2C: Maximum intensity projections from 5 (bud6-3GFP, GFP-bgs4) or 3 (sec6-GFP, sec8-GFP) z-slices spaced by 0.6 μm, and from 14 slices with 0.3 μm spacing for LifeAct-mcherry. Figure 2D: Maximum intensity projections from 3 z-slices spaced by 0.6 μm. 2E: Maximum intensity projections from 11 z-slices spaced by 0.4 μm. Figure 4A: Maximum intensity projections from 7 z-slices spaced by 0.5 μm. Figure 4B: Maximum intensity projections from 5 z-slices spaced by 0.5 μm. Figure 4C: Maximum intensity projections from 5 z-slices spaced by 0.6 μm. Figure 4D: Maximum intensity projections from 3 z-slices spaced by 0.2 μm.

Filamentous fungi imaging was carried out with an inverted epifluorescence microscope (Ti-Eclipse, Nikon) combined with a CMOS camera (Hamamatsu). Hyphae were filmed with a 40x dry objective (CFI Plan Fluor DLL 40X/0.75 NA, Nikon) and a 1.5x magnifier. The microscope was operated with Micro-Manager (Open Imaging).

QUANTIFICATION AND STATISTICAL ANALYSIS

Image analysis

To analyze changes in growth rates and localization of polar factors following growth perturbations, we developed dedicated Matlab scripts [34]. We first segmented cells using the signal from the lectin-labelled cell wall. To this aim, we first smoothed the image with median and Gaussian filters and detected cell edges using the Laplacian of the Gaussian filter. The resultant binary image was then filtered to remove small segments. Given that the signal of the labelled cell wall has a finite thickness, we detected the inner and the outer border of this signal. All spaces in this image were then filled in white except for the spaces between the inner and outer border of the wall, yielding a black band representing the cell wall. Using the watershed algorithm, we finally extracted the whole-cell contour defined as the middle of this band. To compute cell length, we fitted the long axis of the segmented cell

with a polynomial of degree 3. This fit was then used to define a "cell spine" and its length was calculated and used as a measurement for cell length.

The whole-cell contour could then be manipulated using morphological and logical operations to obtain a set of arbitrary regions (tips, membrane, cytoplasm, etc.). The tip regions are for instance shaped as a cut off from the whole-cell mask perpendicular to the cell spine at specific distances along the spine. A segment outside of the cell can be shaped to compute the background.

Fluorescent signals of interest were then extracted from fluorescent images by using a mask based on corresponding sub-regions and are background corrected. Polarization index (PI) was computed by normalizing the background-corrected tip signal with the background-corrected plasma membrane signal:

$$PI = \frac{I_{tip\,raw} - I_{bg}}{I_{plasma\,membrane\,raw} - I_{bg}}$$

Additional image analysis and processing for Figures was done in ImageJ (National Institutes of Health).

Extraction of single cell data

Because of marked rapid changes in cell shape (shrinkage or swelling) upon sorbitol or other treatments, PI and growth rate quantification for single cells was done as an average of data from -15 to 0 min ('pre') and from +10 min to 40 min ('post') relative to treatment, omitting data corresponding to these rapid responses. This calculation was used for the screen results (Figure 3B, 3F, S3C, S3D). Data to compute Figure 1G were extracted in the same manner from experiments in panels 1A, 1C, 1E, 1F and S1D. Data post-treatment from 1E was split into two phases of slowing growth (+10 to +30 min in LatA) and no growth (+35 to +50 min in LatA). To compute the changes in PI or growth rate the difference between pre- and post-treatment values (e.g. $diff_{PI} = PI_{post} - PI_{pre}$) was calculated.

Statistical analysis

Statistical and correlation analyses were carried out using Prism 6 software (GraphPad Software, La Jolla, CA). We used one-way analysis of variance (ANOVA) followed by Dunnett multiple comparisons test or two-tailed, unpaired t-test. Statistically significant difference between groups are *$p < 0.0001$. Linear correlation was analysed by computing the Pearson correlation coefficient.

660 **KEY RESOURCES TABLE**

661

REAGENT or RESOURCE	SOURCE	IDENTIFIER
Experimental Models: *S. pombe* Strains		
h- gpd1::NatMX CRIB-3GFP:ura leu1-32 ura4-D18	This study	AH313
h- CRIB-3GFP:ura leu1-32 ura4-D18 ade-	Lab stocks	NM123
h+ gpd1::NatMX Pcof1-mEGFP-LifeAct:KanMX leu1-32 ura4-D18 ade-	This study	AH371
h+ gpd1::NatMX GFP-syb1:KanMX leu1-32 ura4-D18 ade-	This study	AH409
h+ gpd1::NatMX sec6-GFP:ura4 leu1-32 ura4	This study	AH415
h+ gpd1::NatMX sec8-GFP:ura4 leu1-32 ura4	This study	AH421
h+ gpd1::NatMX bud6-3GFP:KanMX leu1-32 ura4-D18 ade-	This study	AH413
gpd1::KanMX GFP-bgs4-Leu bgs4::ura leu1-32 ura4-D18 ade-	Lab stocks	NM266
h- gpd1::KanMX CRIB-GFP:ura leu1-32 ura4-D18 ade-	Lab stocks	NM434
gpd1::KanMX CRIB-tdTomato:ura sec6-GFP:ura4 leu1-32 ura4-D18	This study	AH477
h- gpd1::KanMX tea1::NatMX CRIB CRIB-3GFP:ura leu1-32 ura4-D18	This study	AH432
h- trk1::KanMX trk2::KanMX CRIB-3GFP:ura	This study	AH229
h+ KanMX6-Pcof1-mEGFP-LifeAct leu- ura- ade-	Chen Lab	QC596
h90 CRIB-3GFP:ura ade6-M216 leu1-32	Lab stocks	DB301
h90 tea1::NatMX CRIB-3GFP:ura leu1-32 ura4-D18	This study	AH242
h90 bud6-3GFP:KanMX leu1-32 ura4-D18	Lab stocks	DB169
h90 bgs4::ura GFP-bgs4:leu leu1-32 ura4-D18	Lab stocks	DB124
h90 CRIB-3GFP:ura Pact1-Lamcherry:leu ade6-M216	Lab stocks	DB337
h90 sec6-GFP:ura leu1-32 ura4-D18 ade-	Lab stocks	DB361
h90 sec8-GFP:ura leu1-32 ura4-D18	Lab stocks	DB362
h90 CRIB-3GFP:ura mCherry-atb2:hph leu1-32 ura4-D18	This study	AH148
ace2::KanMX4 CRIB-3GFP:ura leu1-32 ura4-D18 ade-	This study	AH213
h90 CRIB-GFP:ura bgs4::ura RFP-bgs4:leu leu1-32 ura4-D18	Lab stocks	DB287
h- gpd1::NatMX end4::KanMX CRIB-3GFP:ura leu1-32 ura4-D18	This study	AH332
h+ gpd1::KanMX exo70::NatMX CRIB-3GFP:ura ura4-D18	This study	AH419
h+ gpd1::NatMX for3::KanMX CRIB-3GFP:ura leu1-32 ura4-D18	This study	AH423
h- gpd1::NatMX myo52::ura ars1(BlpI):Padh13:CRIB-3xmCitrine:leu2 leu1-32 ura4-D18 ade-	This study	AH454
gpd1::NatMX ryh1::ura ars1(BlpI):Padh13:CRIB-3xmCitrine:leu2 leu1-32 ura4-D18	This study	AH374
h- gpd1::NatMX mtl2::KanMX CRIB-3GFP:ura leu1-32 ura4-D18 ade-	This study	AH321
h- gpd1::NatMX wsc1::KanMX CRIB-3GFP:ura leu1-32 ura4-D18 ade-	This study	AH320
h+ gpd1::NatMX rgf1::KanMX CRIB-3GFP:ura leu1-32 ura4-D18 ade-	This study	AH346
h- gpd1::NatMX rgf2::KanMX CRIB-3GFP:ura leu1-32 ura4-D18	This study	AH334
h- gpd1::NatMX pck2:leu CRIB-3GFP:ura leu1-32 ura4-D18	This study	AH341
gpd1::NatMX pmk1::KanMX CRIB-3GFP:ura leu1-32 ura4-D18 ade-	This study	AH377
gpd1::NatMX yam8::ura ars1(BlpI):Padh13:CRIB-3xmCitrine:leu2	This study	AH365
h- gpd1::NatMX skb5::KanMX CRIB-3GFP:ura leu1-32 ura4-D18 ade-	This study	AH379

h- gpd1::NatMX rga4::KanMX CRIB-3GFP:ura ura leu1-32 ura4-D18	This study	AH438
gpd1::NatMX gef1::ura ars1(BlpI):Padh13:CRIB-3xmCitrine:leu2 leu1-32 ura4-D18 ade-	This study	AH480
gpd1::NatMX sty1::kanMX ars1(BlpI):Padh13:CRIB-3xmCitrine:leu2 leu1-32 ura4-D18	This study	AH364
h- gpd1::NatMX ssp1::KanMX CRIB-3GFP:ura leu1-32 ura4-D18	This study	AH339
h- gpd1::NatMX tor1::KanMX CRIB-3GFP:ura leu1-32 ura4-D18	This study	AH393
sty1::NatMX for3::KanMX CRIB-3GFP:ura leu1-32 ura4-D18 ade-	This study	AH446
h- *for3::KanMX CRIB-3GFP:ura leu1-32 ura4-D18 ade-*	Lab stocks	NM125
h+ gpd1::KanMX leu1-32:SV40:GFP-atb2[leu1+] ura4-D18 ade-	This study	AH459
h- gpd1::NatMX tea1-3GFP:KanMX leu1-32 ura4-D18 ade-	This study	AH456
h+ gpd1::NatMX leu1-32:GFP-psy1[leu1+] ura4-D18 ade-	This study	AH417
h+ gpd1::NatMX myo52-3GFP:KanMX leu1-32 ura4-D18	This study	AH461
Experimental Models: Filamentous Fungi Strains		
Botrytis cinerea	F. Leclerc lab	LC23
Sordaria macrospora	F. Leclerc lab	LC7
Coprinus cinereus	F. Leclerc lab	LC55
Trametes versicolor	F. Leclerc lab	LC39
Mucor circinelloides	F. Leclerc lab	LC71
Chemicals		
LatrunculinA	Sigma-Aldrich	L5163
Gs-IB_4-Alexafluor647	ThermoFisher	I32450
CK666	Sigma-Aldrich	L0006
Percoll	Sigma-Aldrich	P1644
PDMS kit (Sylgard 184)	Dow Corning	DC184
Oligonucleotides		
Primer: Resistance marker switching forward: CGGATCCCCGGGTTAATTAAGGCG	[44]	MD1
Primer: Resistance marker switching reverse: GAATTCGAGCTCGTTTAAACACTGGATGGCGGCGTTAGTATCG	[44]	MD2
Recombinant DNA		
Vector: pCR2.1-nat	[44]	NEG772014MC

662
663
664
665

SUPPLEMENTAL MOVIE LEGENDS

Movie S1: Changes of the growth rate act upon polarity domain stability. Growth rates were dynamically changed by different means. From left to right: Addition of 0.5 M sorbitol to *gpd1Δ* cells, Reducing glucose content to 0.03% in wild type cells, Treatment with 50 µM Latrunculin A of wild type cells, Addition of 50 mM KCl to *trk1Δtrk2Δ* cells, Addition of 0.5 M sorbitol to *tea1Δgpd1Δ* cells. All strains express CRIB-3GFP. Time elapsed is in h:min. Scale bars are 2 µm.

Movie S2: Growth arrest through mechanical confinement triggers polarity domain destabilization and wandering. Wild-type cells expressing CRIB-3GFP were grown to confinement in microchannels. Time elapsed is in h:min. Scale bar is 2 µm.

Movie S3: Confinement lift induces repolarization and growth. Wild type cells expressing CRIB-3GFP were grown in microchannels to full confinement and two cells were subsequently killed using UV-laser ablation to generate space for neighbors to grow. Arrowheads label reforming stable CRIB domains. Images are maximum intensity projections. Time elapsed is in h:min. Scale bars are 2 µm.

Movie S4: Dynamic adaptation of polarity domains to their mechanical environment. Wild type cells expressing CRIB-3GFP were grown in microchannels. Cells growing from the two opposite ends of the channel and their response upon contact were documented by time-lapse microscopy. Green dashed circle depicts the outline of a dormant spore that did not germinate. Arrowheads label CRIB domains that reorient. Images are maximum intensity projections. Time elapsed is in h:min. Scale bar is 2 µm.